J|A|C|S ARTICLES

Published on Web 08/10/2010

Doped Assemblies of Gold Nanoparticles: Structural and Electronic Properties

Jonathan da Rocha Martins,[†,‡] Ronaldo J. C. Batista,[§] and Hélio Chacham*[,‡]

Departamento de Física, Universidade Federal do Piauí, Campus Ministro Petrônio Portela-Bairro Ininga, 64049-550 Teresina, PI, Brazil, Departamento de Física, ICEX, Universidade Federal de Minas Gerais, CP 702, 30123-970 Belo Horizonte, MG, Brazil, and Universidade Federal de Ouro Preto, Campus Morro do Cruzeiro, 35.400-000 Ouro Preto, MG, Brazil

Received December 7, 2009; E-mail: chacham@fisica.ufmg.br

Abstract: We performed an *ab initio* study of molecular-doped periodic assemblies of ligand-stabilized Au nanoparticles. We found that the most stable dopant positions are near the nanoparticle surfaces, away from the center of interstitial positions. The dopants provide an effective screening mechanism, strongly reducing the nanoparticles charging energies. We also found a linear dependence of the Fermi level with dopant concentration, consistent with recent experiments, up to a critical concentration. For larger concentrations, a new regime is predicted. These features are well reproduced by a simple, analytical model for the material.

Assemblies of ligand-stabilized metal nanoparticles can present peculiar properties that differ from those of bulk materials.[1−4] These assemblies may crystallize in a rich variety of structures,[1,5−9] some of them quite unexpected.[1] The large interstitial voids in these assemblies allow them to be permeated by dopant molecules in a reversible and controllable way, inside electrochemical cells.[2,10] This latter property has been recently used to produce a tunable Schottky barrier between a Au nanoparticle film and a semiconductor surface.[2] Such a chemically tunable electronic device is an example of the technological potential of this new class of nanostructured materials.

In this work, we apply *ab initio* methods to study the changes in the properties of a periodic assembly of Au nanoparticles due to the addition of either donor or acceptor dopant molecules. Specifically, we consider the donor tetrabutylammonium $(C_4H_9)_4N$ molecule and the acceptor hexafluorophosphate (PF_6) molecule. These dopant molecules have been used in recent experiments on Au nanoparticle assemblies,[2] as well as in previous experiments on nanoparticle solutions.[11] To our knowledge, this is the first *ab initio* investigation for this new type of material. We obtain structural and electronic properties, in particular the dependence of the Fermi level E_F[12] with the dopant concentration. We also present an analytical model that is able to reproduce the *ab initio* results, for both the charge transfer and the Fermi level as a function of doping, and is consistent with the electronic structure of the material.

The *ab initio* methodology employed in this work is based on density functional theory (DFT)[13] within the generalized gradient approximation (GGA)[14] for the exchange-correlation functional, as implemented in the SIESTA method.[15,16] The geometries were fully optimized using a conjugate gradient algorithm until all the force components were smaller than 0.05

† Universidade Federal do Piauí.
‡ Universidade Federal de Minas Gerais.
§ Universidade Federal de Ouro Preto.

(1) Kalsin, A. M.; Fialkowski, M.; Paszewski, M.; Smoukov, S. K.; Bishop, K. J. M.; Grzybowski, B. A. *Science* **2006**, *312*, 420.
(2) Boettcher, S. W.; Strandwitz, N. C.; Schierhorn, M.; Lock, N.; Lonergan, M. C.; Stucky, G. D. *Nat. Mater.* **2007**, *6*, 592.
(3) Kovalenko, M. V.; Scheele, M.; Talapin, D. V. *Science* **2009**, *324*, 1417.
(4) Wessels, J. M.; Nothofer, H.-G.; Ford, W. E.; Wrochem, F. V.; Scholz, F.; Vossmeyer, T.; Schroedter, A.; Weller, H.; Yasuda, A. *J. Am. Chem. Soc.* **2004**, *126*, 3349.
(5) Redl, F. X.; Cho, K.-S.; Murray, C. B.; O'Brien, S. *Nature* **2003**, *423*, 968.
(6) Shevchenko, E. V.; Talapin, D. V.; Kotov, N. A.; O'Brien, S.; Murray, C. B. *Nature* **2006**, *439*, 55.
(7) Kalsin, A. M.; Grzybowski, B. A. *Nano Lett.* **2007**, *7*, 1018.
(8) Cheng, W.; Campolongo, M. J.; Cha, J. J.; Tan, S. J.; Umbach, C. C.; Muller, D. A.; Luo, D. *Nat. Mater.* **2009**, *8*, 519.
(9) Ahmed, A. S.; Ryan, K. M. *Adv. Mater.* **2008**, *20*, 4745.
(10) Boettcher, S. W.; Berg, S. A.; Schierhorn, M.; Strandwitz, N. C.; Lonergan, M. C.; Stucky, G. D. *Nano Lett.* **2008**, *8*, 3404.
(11) Pietron, J. J.; Hicks, J. F.; Murray, R. W. *J. Am. Chem. Soc.* **1999**, *121*, 5565.
(12) Throughout this work, E_F will be used as a synonym for the electron chemical potential μ_e, that is, the term will be used for finite temperatures as well.
(13) Kohn, W.; Sham, L. J. *Phys. Rev.* **1965**, *140*, A1133.
(14) Perdew, John P.; Burke, K.; Ernzerhof, M. *Phys. Rev. Lett.* **1996**, *77*, 3865.
(15) Soler, J. M.; Artacho, E.; Gale, J. D.; Garcia, A.; Junquera, J.; Ordejon, P.; Sanchez-Portal, D. *J. Phys.: Condens. Matter* **2002**, *14*, 2745.
(16) We make use of norm-conserving scalar relativistic pseudopotentials[17] in the Kleinman-Bylander nonlocal form.[18] The pseudopotentials were generated from atomic valence configurations $5d^{10}6s^1$, $3s^23p^4$, $2s^22p^2$, and $1s^1$ of Au, S, C, and H, respectively, with core radii (in units of a_0) 2.32 (Au), 1.69 (S), 1.25 (C), and 1.25 (H). Linear combinations of numerical pseudoatomic orbitals of finite range consisting of double-ζ radial functions per angular momentum plus polarization orbitals were employed as a basis set. The range of each atomic orbital was determined by a common energy shift of 0.01 Ry.[19,20] The fineness of the real space grid integration was defined by an energy cutoff (150 Ry) of the plane wave that can be represented in it without aliasing.[21]
(17) Troullier, N.; Martins, J. L. *Phys. Rev. B* **1991**, *43*, 1995.
(18) Kleinman, L.; Bylander, D. M. *Phys. Rev. Lett.* **1982**, *48*, 1425.
(19) Sankey, O. F.; Niklewski, D. J. *Phys. Rev. B* **1989**, *40*, 3979.
(20) Junquera, J.; Paz, O.; Sánchez-Portal, D.; Artacho, E. *Phys. Rev. B* **2001**, *64*, 235111.
(21) Moreno, J.; Soler, J. M. *Phys. Rev. B* **1992**, *45*, 13891.

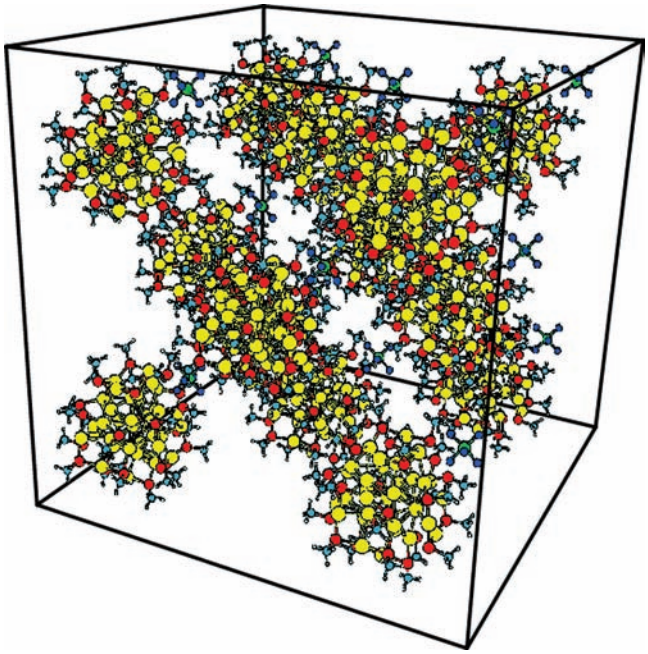

Figure 1. Fcc assembly of $Au_{38}(SCH_3)_{24}$ **1** nanoparticles doped with PF_6.

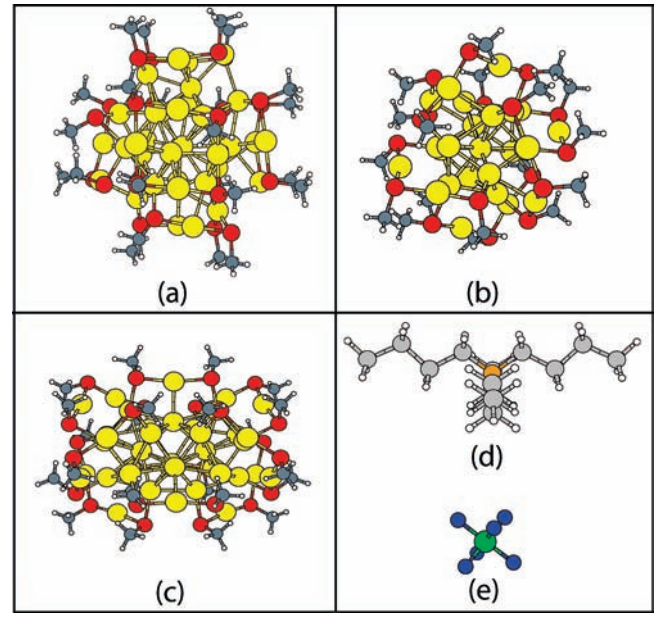

Figure 2. Structures of (a) $Au_{38}(SCH_3)_{24}$ **1** of Garzon et al.,[27] (b) $Au_{25}(SCH_3)_{18}$ of Akola et al.,[28] (c) $Au_{38}(SCH_3)_{24}$ **2** of Pei et al.,[26] (d) tetrabutylammonium (donor molecule), and (e) PF_6 (acceptor molecule).

eV/Å. The methodology described above has been tested in a previous work[22] and applied to investigate 2D lattices of Au nanoparticles[23] and isolated Au nanoparticles.[24]

As a first model for an assembly of ligand-stabilized Au nanoparticles, we consider methylthiol-capped nanoparticles periodically assembled in a face-centered cubic (fcc) structure, as shown in Figure 1. Our choice of structure was based on recent experimental results on the crystallization of Au nanoparticles into fcc lattices.[25] We consider three distinct models for the methylthiol-capped nanoparticles: two isomer structures of $Au_{38}(SCH_3)_{24}$[26,27] and one specific structure of $Au_{25}(SCH_3)_{18}$.[28] We will refer to the amorphous Au_{38} structure of Garzon et al.,[27] shown in Figure 2a, as $Au_{38}(SCH_3)_{24}$ **1** and the lowest-energy prolate structure of Pei et al.,[26] shown in Figure 2c, as $Au_{38}(SCH_3)_{24}$ **2**. The $Au_{25}(SCH_3)_{18}$ structure obtained by Akola et al.[28] is shown in Figure 2b. In the three nanoparticle models, the resulting S−Au−S bonds are quasi-linear, consistent with experimental observations.[29] Motivated by recent experimental work,[2] we also consider that the nanoparticle crystals can be doped with either the PF_6 (acceptor) or the tetrabutylammonium (donor) molecule, shown in Figure 2d and e, respectively.

Let us first discuss the structural properties of the molecular-doped nanoparticle assemblies. More specifically, we compare

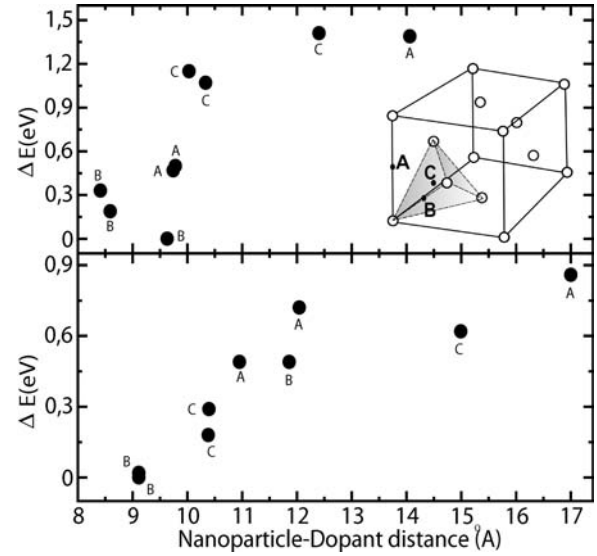

Figure 3. Relative energy of doped assemblies of $Au_{38}(SCH_3)_{24}$ **1** as a function of the distance between dopant and nanoparticle centers. (Top) PF_6 dopant. (Bottom) Tetrabutylammonium dopant. Each point is labeled A, B, or C corresponding to linear paths from the center of the nanoparticle to the sites **A**, **B**, and **C**. Insert: schematic positions of the fcc assembly. Black dots, interstitial positions. White circles, nanoparticle positions.

the energetic stability of the dopant molecules at different sites of the fcc assembly shown in Figure 1. We consider the three types of interstitial sites of the fcc lattice, shown in the inset of Figure 3. Site **A** is the octahedral interstitial site, **B** is the bond-centered interstitial site, and **C** is the tetrahedral interstitial site. We considered, as initial geometric configurations, that the geometrical center of the dopant molecules can be placed along the paths **OA**, **OB**, and **OC**, where the position **O** is the center of the nanoparticle at the lower left of the inset of Figure 3. We then optimized these structures, starting from each initial position, until the remanent forces were less than 0.05 eV/Å. The resulting total energies, for the fcc lattice of $Au_{38}(SCH_3)_{24}$ **1** nanoparticles, are shown in Figure 3 for both dopants as a

(22) Batista, R. J. C.; Mazzoni, M. S. C.; Ladeira, L. O.; Chacham, H. *Phys. Rev. B* **2005**, *72*, 085447.
(23) Batista, R. J. C.; Mazzoni, M. S. C.; Garzon, I. L.; Beltran, M. R.; Chacham, H. *Phys. Rev. Lett.* **2006**, *96*, 116802.
(24) Batista, R. J. C.; Mazzoni, M. S. C.; Chacham, H. *Nanotechnology* **2010**, *21*, 065705.
(25) Abécassis, B.; Testard, F.; Spalla, O. *Phys. Rev. Lett.* **2008**, *100*, 115504.
(26) Pei, Y.; Gao, Y.; Zeng, X. C. *J. Am. Chem. Soc.* **2008**, *130*, 7830.
(27) Garzón, I. L.; Rovira, C.; Michaelian, K.; Beltrán, M. R.; Ordejón, P.; Junquera, J.; Sánchez-Portal, D.; Artacho, E.; Soler, J. M. *Phys. Rev. Lett.* **2000**, *85*, 5250.
(28) Akola, J.; Walter, M.; Whetten, R. L.; Hakkinen, H.; Gronbeck, H. *J. Am. Chem. Soc.* **2008**, *130*, 3756.
(29) Jadzinsky, P. D.; Calero, G.; Ackerson, C. J.; Bushnell, D. A.; Kornberg, R. D. *Science* **2008**, *318*, 430.

function of the distance between the dopant molecule and the nanoparticle center. The top and the bottom panels of Figure 3 show the results for the nanoparticle crystal doped with PF_6 and tetrabutylammonium, respectively.

The results of the top panel of Figure 3 indicate that the most stable positions of the PF_6 dopant molecule are near the nanoparticle surface, along the bond-centered (**OB**) direction. Positions near the octahedral (**A**) and the tetrahedral (**C**) interstitial sites, the farthest away from the nanoparticle surface, are the least stable ones. The bottom panel of Figure 3 shows similar results for the tetrabutylammonium dopant molecule. Overall, these results strongly indicate that both dopants have the most stable positions near the nanoparticle surfaces, preferably along the path between first-neighbor particles. The large energy difference between the positions near the nanoparticle surface and those near the interstitial positions (of the order of 1 eV) also suggest that the diffusion of the dopants should follow paths near the nanoparticles surfaces (i.e., "around" the particles), followed by hopping along the paths between first-neighbor nanoparticles.

Let us now consider the electronic properties of the molecular-doped nanoparticle assemblies. In experiments with assemblies inside electrochemical cells,[2] one of the measured quantities is the Fermi level E_F established at the nanoparticle assembly through the (tunable) doping level. In our calculations, the occupation of the Kohn−Sham eigenvalues is given by a Fermi−Dirac distribution at $T = 174$ K with a value of E_F that results in a neutral unit cell (nanoparticle + dopants). This calculated E_F is the quantity that would be the closest related to the one in the experiments. Our calculations are performed for an infinite, periodic system. Therefore, it is necessary to define a common energy reference for the assemblies with different number of dopants. We have chosen two possible energy references, which lead to consistent results for the changes of E_F with doping within an uncertainty of 0.16 eV. One is the 2s eigenvalue of a He atom placed at a position inside the unit cell, such that there is no overlap between its basis set and the nanoparticle or the dopant molecules basis set. Our second choice for the energy reference is the average Kohn−Sham potential.

The change in the Fermi level E_F of the $Au_{38}(SCH_3)_{24}$ **1** fcc assembly due to doping is shown in the top panel of Figure 4. The figure shows that, upon doping with up to two molecules/cell, the Fermi level changes in an approximately linear way with either acceptor or donor doping, decreasing with acceptor doping and increasing with donor doping. This behavior is consistent with the experimental observations.[2] The variation of E_F is due to charge transfer between nanoparticle and dopants. This charge transfer was calculated through Mulliken population analysis and is shown in the bottom panel of Figure 4 as the excess of charge in the nanoparticle due to doping. The figure shows that, up to a doping level of two molecules per nanoparticle, each donor (acceptor) molecule donates (receives) nearly one electronic unit charge (e) to (from) the nanoparticle.

The structure that we considered so far for the nanoparticle assembly is a close-packed one. To investigate the possible effects of less dense, possibly anisotropic structures on the properties of Au nanoparticle assemblies, let us also consider a single layer of $Au_{38}(SCH_3)_{24}$ **1** nanoparticles placed at the sites of a 2D triangular lattice. Such 2D assemblies have been experimentally obtained and investigated.[30] The calculated

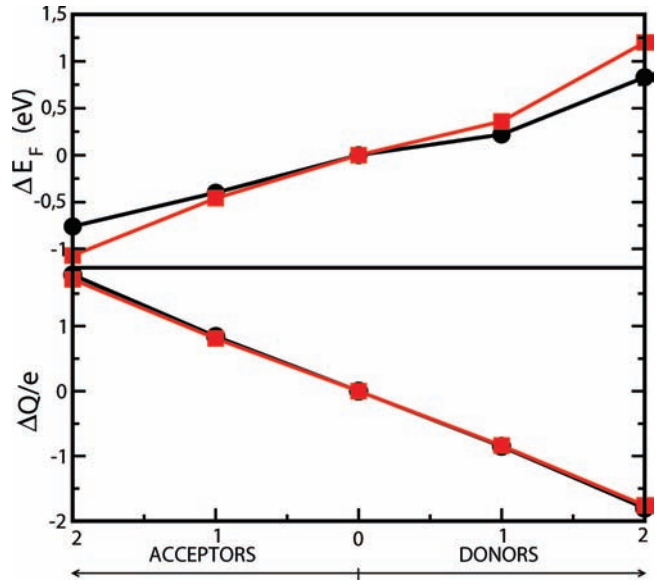

Figure 4. (Top) Variation of E_F of assemblies of $Au_{38}(SCH_3)_{24}$ **1** due to doping with either PF_6 (acceptor) or tetrabutylammonium (donor). (Bottom) Excess of charge on each nanoparticle due to doping. Horizontal axis: number of acceptor/donor molecules per particle. Circles indicate the results for the fcc assembly, and squares are results for the single-layer, triangular lattice.

change in E_F for the 2D assembly due to doping is shown in the top panel of Figure 4, together with the results for the fcc assembly. A comparison between the results for the fcc and the 2D assemblies shows that the main effect due to the reduced dimensionality is the increase, by a factor of about 1.4, of the slope of E_F versus doping. A possible explanation for that effect is a less effective dielectric screening in the 2D assembly, as compared to the fcc one. Such explanation is also consistent with an even larger slope (in the low-doping regime) for the case of an isolated nanoparticle, to be discussed below.

The exchange of electrons between nanoparticles and dopants, observed above for a low concentration of dopants, should saturate in the case of higher concentrations. In order to address the saturation regime, we consider a molecular model in which an isolated nanoparticle is surrounded by up to 12 PF_6 molecules. This molecular model prevents the overlap between dopants at neighboring nanoparticles and does not require the use of a common energy reference. The model also allows us to identify dopant screening effects and to distinguish them from bulk screening. The results of our *ab initio* calculations for this molecular model are shown in Figure 5 for $Au_{38}(SCH_3)_{24}$ **1**, in Figure 6 for $Au_{38}(SCH_3)_{24}$ **2**, and in Figure 7 for $Au_{25}(SCH_3)_{18}$. The bottom panel of Figure 5 indicates that the nearly integer charge tranfer from the dopant molecules to the nanoparticle holds up to a critical number of $N_C \approx 4$ PF_6 molecules per particle for $Au_{38}(SCH_3)_{24}$ **1**. Above that, only a fractional charge (of about 0.26 e) is transferred from each additional dopant to the nanoparticle. A similar behavior, also shown in Figure 5, is obtained for the behavior of E_F as a function of the number N of dopant molecules. The figure shows that E_F varies linearly with N up to the same critical N_C, with a slope of smaller magnitude for larger values of N. Similar trends for charge transfer and E_F as functions of N were obtained for $Au_{38}(SCH_3)_{24}$ **2** and $Au_{25}(SCH_3)_{18}$ and are shown in Figures 6 and 7. In an experimental setup, such change in the charging behavior of nanoparticles could be identified as a reduction of the chemical potential spacing between successive nanoparticle charging

(30) Ulman, A. *Chem. Rev.* **1996**, *96*, 1533.

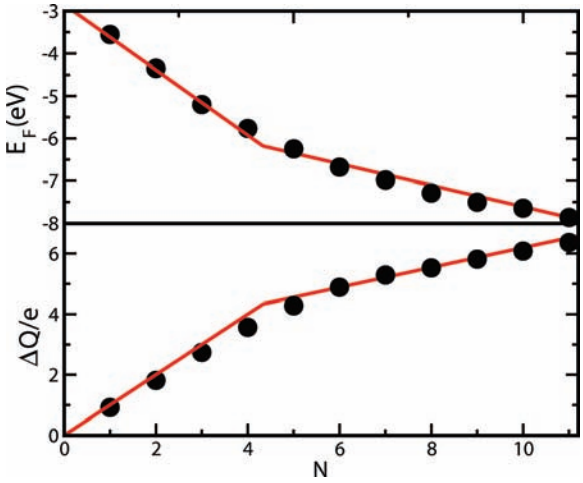

Figure 5. Fermi level (top) and charge (bottom) of isolated $Au_{38}(SCH_3)_{24}$ **1** surrounded by a varying number (N) of PF_6 molecules. Lines: eqs 3 (top) and 2 (bottom).

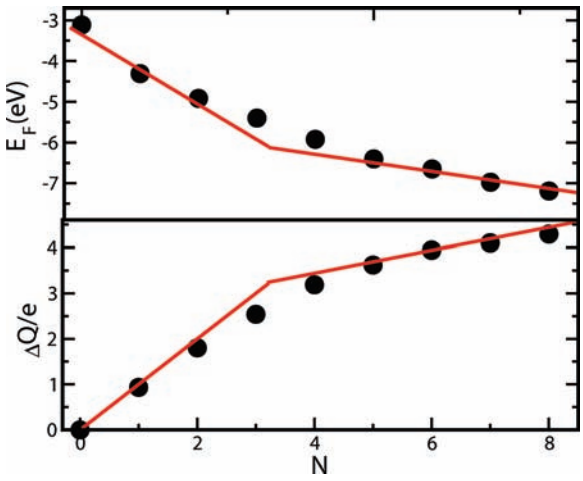

Figure 6. Fermi level (top) and charge (bottom) of isolated $Au_{38}(SCH_3)_{24}$ **2** surrounded by a varying number (N) of PF_6 molecules. Lines: eqs 3 (top) and 2 (bottom).

events, in the regime of large (positive or negative) applied potentials. Spacing reductions of this type have indeed been observed in experiments on nanoparticle solutions.[31,32]

Why do the nanoparticle charge and Fermi levels depict similar (or more precisely, specular) behaviors as a function of the number N of dopant molecules, as shown in Figures 5, 6, and 7? To address this question, let us consider the density of states (DOS) of the $Au_{38}(SCH_3)_{24}$ **1** nanoparticle crystal doped with one PF_6 (acceptor) molecule per nanoparticle, shown in Figure 8. Two characteristic features can be seen in the figure: first, the nanoparticle occupied valence states fall between −12 and −3 eV; second, the occupied states of the acceptor molecule fall several eV below E_F.

As more acceptor molecules are added to the assembly, the nanoparticle becomes more positively charged, causing an energy downshift of the nanoparticle occupied states relative to acceptor states. Eventually, for higher doping, the highest

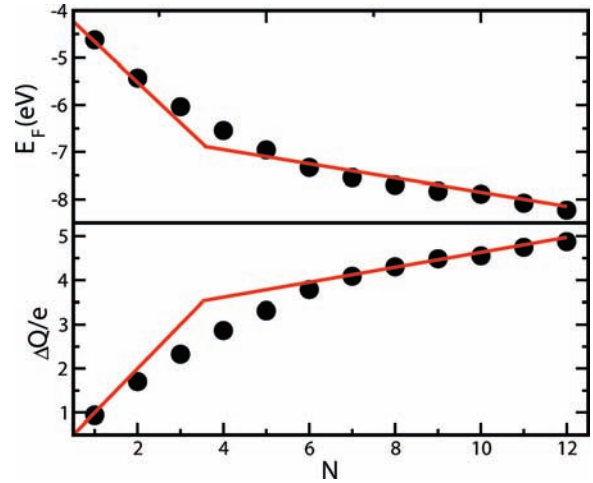

Figure 7. Fermi level (top) and charge (bottom) of isolated methylthiolated Au_{25} surrounded by a varying number (N) of PF_6 molecules. Lines: eqs 3 (top) and 2 (bottom).

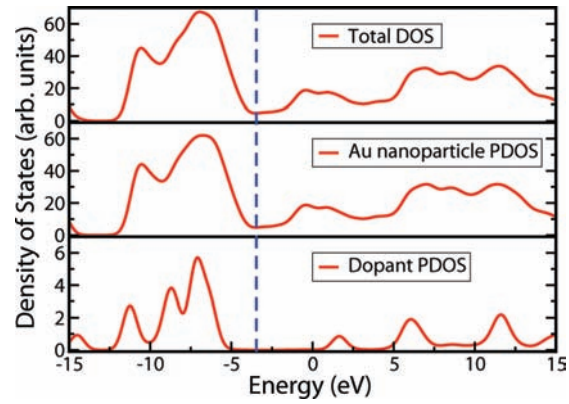

Figure 8. (Top) Density of states (DOS) of the $Au_{38}(SCH_3)_{24}$ **1** fcc assembly doped with one PF_6 molecule per particle. (Middle) Projected at the nanoparticle. (Bottom) Projected at PF_6.

ocupied states of both subsystems (nanoparticles and dopants) would become degenerate, initiating the new doping regime for $N > N_C$.

In view of the above, we propose a density functional model that contains the major features of the electronic structure described in the preceding paragraph and that reproduces quantitatively the results of Figures 5, 6, and 7. In this model, the total energy of an assembly with N dopant molecules per nanoparticle is given by

$$E = \varepsilon_1 n_1 + \varepsilon_2 n_2 + \frac{1}{2}U_1 n_1^2 + \frac{1}{2}U_2 n_2^2 \qquad (1)$$

where n_1 and n_2 are the number of additional electrons (where n_1, n_2, and N are negative in the case of acceptor-doped system) on the nanoparticle and on the dopant molecules, respectively. The charge neutrality of the system is imposed by the condition $n_1 + n_2 = N$. ε_1 and ε_2 are chemical potentials for the nanoparticle and the dopant molecules, respectively. U_1 and U_2 represent on-site electron−electron repulsion terms. The minimization of eq 1 with respect to n_1 results in

$$n_1 = \begin{cases} N & |N| < |N_C| \\ \dfrac{\varepsilon_2 - \varepsilon_1}{U_1 + U_2} + \dfrac{U_2}{U_1 + U_2}N & |N| > |N_C| \end{cases} \qquad (2)$$

(31) Hicks, J. F.; Miles, D. T.; Murray, R. W. *J. Am. Chem. Soc.* **2002**, *124*, 13322.
(32) Hicks, J. F.; Templeton, A. C.; Chen, S.; Sheran, K. M.; Jasti, R.; Murray, R. W. *Anal. Chem.* **1999**, *71*, 3703.

where $N_C = (\varepsilon_2 - \varepsilon_1)/U_1$. We also obtain the Fermi level $E_F = \mu = dE/dN$ as

$$E_F = \begin{cases} \varepsilon_1 + U_1 N & |N| < |N_C| \\ \varepsilon_2 + \dfrac{U_1 U_2}{U_1 + U_2}(N - N_C) & |N| > |N_C| \end{cases} \quad (3)$$

Equations 2 and 3 are plotted in Figure 5 for $Au_{38}(SCH_3)_{24}$ **1** with the set of parameters $\varepsilon_1 = -2.85$ eV, $\varepsilon_2 = -6.18$ eV, $U_1 = 0.770$ eV, and $U_2 = 0.375$ eV. The same equations are plotted in Figure 6 for $Au_{38}(SCH_3)_{24}$ **2** with the set of parameters $\varepsilon_1 = -3.35$ eV, $\varepsilon_2 = -6.15$ eV, $U_1 = 0.860$ eV, and $U_2 = 0.290$ eV. In both cases, eqs 2 and 3 provide good agreement with the *ab initio* results. These equations are also plotted in Figure 7 for $Au_{25}(SCH_3)_{18}$ with the set of parameters $\varepsilon_1 = -3.80$ eV, $\varepsilon_2 = -6.87$ eV, $U_1 = 0.860$ eV, and $U_2 = 0.176$ eV. In this case, eqs 2 and 3, which result from the classical model of eq 1, show larger deviations from the *ab initio* calculations, suggesting the existence of stronger quantum effects, not included in the model, in this smaller nanoparticle. A comparison between Figures 5 and 7 suggests that the transition between the low- and the high-coverage behavior becomes sharper and more consistent with the classical model of eq 1, as the nanoparticle size increases.

Among the parameters of the model of eq 1, U_1 is one that can be compared with experiments. Namely, U_1 is the chemical potential spacing between successive nanoparticle charging events, in the regime of small charge (see eq 3), which can be obtained experimentally.[2,11,31] We found that U_1 is a strongly screened quantity. A first screening mechanism, a "dopant" one, results from the fact that, for each additional unit charge in the nanoparticle, an extra dopant ion is placed around it to ensure charge neutrality. For $Au_{38}(SCH_3)_{24}$ **1**, this strongly reduces U_1 from the "bare" value of 2.0 eV (for the undoped nanoparticle) to the dopant screened value of 0.77 eV obtained in our model. A second screening mechanism, a "bulk" one, results from packing the nanoparticles into the assembly. This further reduces the screened U_1 from 0.77 to 0.38 eV, the latter being the charging energy spacing in Figure 4. These screening effects result in an effective dielectric constant $\varepsilon = U_1^{bare}/U_1^{screened} = 5.3$. This can be compared with the result $\varepsilon = 6.9$ in recent experiments[2] for assemblies of Au nanoparticles with diameters of the order of 2.1 nm, twice as large as that of $Au_{38}(SCH_3)_{24}$ **1** (1.0 nm). Considering that the capacitance of a metallic sphere scales linearly with its diameter D, the product U_1D should be nearly constant. In this sense, our calculated result for this product, $U_1D = 0.38$ eV.nm, is consistent with the experimental value of $U_1D = 0.40$ eV.nm.[2]

Acknowledgment. We wish to acknowledge the agencies CNPq and FAPEMIG for financial support. We also thank R. W. Nunes for a critical reading of the manuscript.

JA910335H